Nat. Hazards Earth Syst. Sci. Discuss., 2, 1–25, 2014
www.nat-hazards-earth-syst-sci-discuss.net/2/1/2014/
doi:10.5194/nhessd-2-1-2014

Natural Hazards and Earth System Sciences
Open Access
Discussions

Developing fragility functions for the areas affected by the 2009 Samoa earthquake and tsunami

H. Gokon[1], S. Koshimura[2], K. Imai[2], M. Matsuoka[3], Y. Namegaya[4], and Y. Nishimura[5]

[1]Graduate School of Engineering, Tohoku University, Japan
[2]International Research Institute of Disaster Science, Tohoku University, Japan
[3]Interdisciplinary Graduate School of Science and Engineering, Tokyo Institute of Technology, Japan
[4]Geological Survey of Japan, National Institute of Advanced Industrial Science and Technology, Japan
[5]Institute of Seismology and Volcanology, Graduate School of Science, School of Science, Hokkaido University, Japan

Received: 7 November 2013 – Accepted: 18 November 2013 – Published: 2 January 2014

Correspondence to: H. Gokon (gokon@geoinfo.civil.tohoku.ac.jp)

Published by Copernicus Publications on behalf of the European Geosciences Union.

Abstract

Fragility functions in terms of flow depth, flow velocity and hydrodynamic force are developed to evaluate structural vulnerability in the areas affected by the 2009 Samoa earthquake and tsunami. First, numerical simulations of tsunami propagation and inundation are conducted to reproduce the features of tsunami inundation. To validate the results, flow depths measured in field surveys and waveforms measured by Deep-ocean Assessment and Reporting of Tsunamis (DART) gauges are utilized. Next, building damage is investigated by manually detecting changes between pre- and post-tsunami high-resolution satellite images. Finally, the data related to tsunami features and building damage are integrated using GIS, and tsunami fragility functions are developed based on the statistical analyses.

1 Introduction

On 29 September 2009 (UTC), an earthquake doublet of magnitudes 8.0 and 7.9 and a subsequent tsunami struck the Samoan Islands and Tonga (Beavan et al., 2010; Lay et al., 2010). After the event, an International Tsunami Survey Team (ITST) was deployed, and the mechanism and impacts of this earthquake and tsunami have been studied in terms of geology, geophysics, seismology, sociology and engineering (Apotsos et al., 2011; Dudley et al., 2011; Jaffe et al., 2011; Lamarche et al., 2010; Okal et al., 2011; Roeber et al., 2010; van ZijlldeJong et al., 2011; Wilson et al., 2011). Okal et al. (2010) surveyed the tsunami run-up height at nearly 400 points and found maximum run-up heights of 17.6 m at Poloa in American Samoa and 22.4 m at Tafahi in northern Tonga. The tsunami caused nearly 200 deaths in independent Samoa, American Samoa, and Tonga (Okal et al., 2010; Dudley et al., 2011).

To construct communities that will be resilient to destructive tsunami disasters, it is necessary to evaluate not only the mechanism and impacts of the disaster but also the vulnerability of the coastal region. “Tsunami fragility functions” have been developed

NHESSD

2, 1–25, 2014

to evaluate the structural vulnerability of coastal communities to tsunami disasters and have been tested on several tsunami events (Koshimura et al., 2009b, 2010; Mas et al., 2012; Reese et al., 2011; Suppasri et al., 2011, 2012). Tsunami fragility functions express the relationship between the proportional damage to buildings, vegetation, or human life and the tsunami-inundation features, such as flow depth, current velocity and hydrodynamic force. These parameters are described quantitatively, making it possible to distinguish safe and potentially damaged zones. For the 2009 Samoa event, only Reese et al. (2011) have developed fragility functions using surveyed data. Fragility functions are developed probabilistically; to more accurately evaluate the vulnerability of affected areas, fragility functions should be proposed from several points of view.

The primary objective of this study is to develop tsunami fragility functions by integrating tsunami-inundation features with the spatial distribution of building damage using GIS. To derive the tsunami-inundation features, a detailed consideration of the tsunami-source model and numerical modeling of the tsunami inundation are conducted. Different grades of building damage are then interpreted using pre- and post-tsunami high-resolution satellite images. The tsunami-simulation and building-damage results are verified using field-survey data. Finally, the data related to tsunami features and building damage are integrated using GIS, and tsunami fragility functions are developed based on the statistical analyses.

2 Post-tsunami field survey

The study area encompassed Pago Pago, Leone, Poloa, and Amanave, American Samoa (Fig. 1). Two field surveys were conducted, from 5 to 8 October 2009 and from 23 to 26 July 2010. In the first survey, flow depth, run-up height, and the inundation-area boundary were investigated, and each building in the affected areas was photographed using a GPS-equipped camera (Koshimura et al., 2010; Namegaya et al., 2010). In the second survey, precise land elevations were measured at Pago Pago, Leone, Poloa and Amanave, American Samoa, using a Magellan kinematic GPS (ProMark3). This

NHESSD
2, 1–25, 2014

kinematic GPS is highly accurate; if sufficient satellite coverage exists, positional accuracies of ±20 mm (horizontal) and ±30 mm (vertical) can be achieved.

3 Tsunami numerical simulations

In contrast to most earthquakes, the 2009 Samoa earthquake involved the nearly simultaneous rupture of distinct faults with different geometries (Beavan et al., 2010; Lay et al., 2010). To understand the mechanism and impacts of the 2009 Samoa earthquake and tsunami, some researchers have conducted numerical simulations of the tsunami (Beavan et al., 2010; Didenkulova, 2013; Fritz et al., 2011; Roeber et al., 2010). Several hypotheses related to a series of earthquake doublets have been proposed; however, no consensus has been reached regarding the earthquake seismology. Here, to understand the tsunami-generation mechanism and to reproduce the tsunami-inundation behavior more precisely, two types of numerical simulations were conducted. First, numerical simulations of far-field tsunami propagation and reverse propagation were conducted, and the parameters of the ruptured faults were studied to reproduce the waveforms measured by the Deep-ocean Assessment and Reporting of Tsunamis (DART) network. Second, the tsunami-inundation behavior was simulated to investigate the flow depth, current velocity and hydrodynamic force at Pago Pago, Leone, Poloa and Amanave, American Samoa.

3.1 Understanding the tsunami-generation mechanism

To understand the tsunami-generation mechanism, the far-field tsunami propagation was simulated to reproduce the waveforms observed at DART gauges 51525, 51426 and 54401. The simulations were conducted according to the fault parameters of Beavan et al. (2010).

Initially, the fault-rupture areas related to tsunami generation were roughly estimated based on reverse-propagation analyses from each DART gauge. For outer-rise fault

NHESSD
2, 1–25, 2014

rupture, the rise time was fixed at 60 s, and the time of rupture onset was assumed to be 17:48 on 29 September 2009 (UTC). For fault rupture on the interface, 20 sets of rise times ranging from 0 to 600 s at 30 s intervals were examined. The wave forms derived from these outer-rise and interface rise times were combined with different times of initial fault rupture ranging from 10 min before to 10 min after earthquake generation.

Despite numerous attempts using trial and error, the waveforms of the DART gauges located north and south of the epicenter could not be reproduced simultaneously using the original fault parameters of Beavan et al. (2010). To find a set of fault parameters that would simultaneously reproduce the northward and southward DART waveforms, the fault parameters were modified slightly based on the distribution of aftershocks during the week after the initial earthquake generation while satisfying the coincidence of the seismic moment, as shown in Table 1.

These simulations showed that the waveforms of the three DART gauges were reproduced well if the fault rupture on the interface started three minutes before the fault rupture on the outer rise. The simulated and observed DART waveforms are shown in Fig. 2.

3.2 Tsunami-inundation simulations

3.2.1 Digital bathymetry and topography grid model

For the numerical simulation of tsunami inundation at Pago Pago, Leone, Poloa and Amanave, Tutuila Island, American Samoa, the model was based on a set of non-linear shallow-water equations with bottom friction in the form of Manning's formula according to land use. The equations were discretized according to the staggered leapfrog finite-difference scheme. To develop the computational grids for the numerical model, we used a digital-bathymetry grid derived from the GEBCO 30 s bathymetry dataset and an NOAA-NGDC topography grid with a 3-arcsec Digital Elevation Model (DEM) of American Samoa.

NHESSD
2, 1–25, 2014

To model tsunami inundation in densely populated zones, we applied low resistance with a composite equivalent roughness coefficient based on the land use and building conditions (Aburaya and Imamura, 2002). In the equivalent roughness coefficient, we incorporated building density by generating building-footprint data from the pre-tsunami QuickBird satellite images acquired on 15 April 2007 and 24 September 2009.

3.2.2 Tsunami source model

The fault proposed above accurately reproduced the DART waveforms but did not accurately reproduce the tsunami-inundation behavior in American Samoa. To reproduce the observed tsunami behavior at Pago Pago, Leone, Poloa and Amanave, tsunami-inundation simulations were conducted according to the fault parameters of Beavan et al. (2010). An example of a tsunami source model is shown in Fig. 4a, and the simulated tsunami waveforms at the DART gauges according to Beavan et al. (2010) and corresponding fault parameters are shown in Table 2 and Fig. 3.

3.3 Numerical modeling of tsunami inundation

We modified the fault slip to reproduce the inundation-area boundary and flow depth at each locality. At Pago Pago, we measured several tsunami-inundation features, such as flow depth and run-up height. These data were used to validate the numerical simulations based on Aida (1978). According to Aida (1978), the geometric mean K and geometric standard deviation κ derived from surveyed data can be used to evaluate the reproducibility of numerical simulations of tsunami events.

Aida's K and κ are defined as follows:

$$\log K = \frac{1}{n}\sum_{i=1}^{n} \log K_i \quad (1)$$

NHESSD
2, 1–25, 2014

$$\log\kappa = \sqrt{\frac{1}{n}\sum_{i=1}^{n}(\log K_i)^2 - (\log K)^2} \quad (2)$$

$$K_i = \frac{R_i}{H_i} \quad (3)$$

where R_i and H_i are the measured and modeled values of inundation height/depth at point i, respectively. K is defined as the geometrical mean of K_i and κ as the deviation or variance from K, and these indices are used as criteria to validate the model by comparing the modeled and measured tsunamis. For Pago Pago, $K = 0.97$ and $\kappa = 1.13$ were obtained. These values satisfy the adequacy criteria for tsunami numerical modeling established by the Japan Society of Civil Engineers ($0.95 < K < 1.05$, $\kappa < 1.45$). For Leone, Poloa and Amanave, due to the lack of measured points, the numerical simulation was validated based on the inundation-area boundaries measured in the field survey (Jaffe et al., 2010; Koshimura et al., 2009a). Examples of the simulated results in terms of flow depth are shown in Fig. 4b–e.

4 Interpretation of building damage

Building damage was manually interpreted using pre- and post-tsunami high-resolution satellite images in a GIS framework. An Ikonos satellite image acquired on 15 April 2007 and published by the GeoEye company in the US and a QuickBird satellite image acquired on 24 September 2009 and published by the Digital Globe company in the US were utilized as pre-event images. QuickBird satellite images acquired on 29 September 2009, 02 October 2009, and 02 November 2009 and published by the Digital Globe company were utilized as post-event images.

A total of 451 buildings in the inundated areas were investigated using remote-sensing technology and field surveys. Building damage was classified into four degrees: “Survived”, “Major damage”, “Collapsed”, and “Washed away” (Fig. 5 left), ac-

NHESSD
2, 1–25, 2014

cording to Miura et al. (2006). These data were validated based on the photos of each building taken using a GPS-equipped camera during the field survey. The damage-interpretation results are shown in Fig. 5 right and Table 3.

5 Developing tsunami fragility functions

5.1 Tsunami fragility functions

Fragility functions provide a new method to estimate structural damage and casualties due to tsunami events. These functions are developed through an integrated approach using numerical simulations of tsunami inundation and GIS analyses and are expressed as the probabilities of structural damage or death rates with respect to the hydrodynamic features of tsunami inundation, such as flow depth, current velocity and hydrodynamic force (Koshimura et al., 2009b).

According to Koshimura et al. (2009b), fragility functions are defined by the following formulas:

$$P_D(x) = \Phi\left[\frac{x-\mu}{\sigma}\right] \tag{4}$$

$$= \int_{-\infty}^{x} \frac{1}{\sqrt{2\pi}\sigma} \exp\left(-\frac{(t-\mu)^2}{2\sigma^2}\right) \mathrm{d}t \tag{5}$$

$$P_D(x) = \Phi\left[\frac{\ln x - \lambda}{\xi}\right] \tag{6}$$

$$= \int_{-\infty}^{x} \frac{1}{\sqrt{2\pi}\xi t} \exp\left(-\frac{(\ln t - \lambda)^2}{2\xi^2}\right) \mathrm{d}t \tag{7}$$

NHESSD
2, 1–25, 2014

where Φ is the standardized normal (lognormal) distribution function, x is a hydrodynamic feature of the tsunami (e.g., flow depth, current velocity or hydrodynamic force), and, μ and σ, (λ and ξ) are the mean and standard deviation of x (ln$x$), respectively.

Throughout the regression analysis, the parameters shown in Table 4 were used to obtain the best fit for fragility functions with respect to the flow depth (m), maximum current velocity (m s^{-1}) and hydrodynamic force on structures per unit width (kN m^{-1}). Here, the hydrodynamic force acting on a structure is defined as the drag force per unit of width:

$$F = \frac{1}{2} C_D \rho \mu^2 D \tag{8}$$

where C_D is the drag coefficient ($C_D = 1.0$ for simplicity), ρ is the density of water ($= 1000\,kg\,m^{-3}$), μ is the current velocity ($m\,s^{-1}$), and D is the flow depth (m).

To develop the tsunami fragility functions, the four damage levels were grouped into two classes, "Destroyed" and "Undestroyed". "Destroyed" buildings were defined as structurally damaged buildings and included three damage levels: "Washed away", "Collapsed", and "Major damage". "Undestroyed" buildings were defined as structurally non-damaged buildings that were classified as "Survived" in the building-damage interpretation.

The resulting fragility functions, which are presented in Fig. 6, show the relationships between damage probabilities and the hydrodynamic features of tsunami inundation in American Samoa.

5.2 Discussion

The fragility function of flow depth, shown in Fig. 6a, begins to increase as the flow depth exceeds 1 m, and 80 to 90 % of buildings are destroyed as the flow depth reaches 6 m. This sudden rise in damage at a relatively low flow depth implies the vulnerability of this coastal region, which is likely to experience high water levels during tsunami events due to its ria coasts.

NHESSD
2, 1–25, 2014

The fragility function of current velocity, shown in Fig. 6b, rises steeply at a low current velocity of less than 2 m s^{-1} and rises gently at current velocities greater than 2 m s^{-1}. The fragility function of hydrodynamic force, shown in Fig. 6c, also rises steeply at low hydrodynamic forces and rises gently at forces greater than 5 kN m^{-1}. Compared to the flow-depth fragility function, these two functions show the variation among the interpreted points. A closer examination showed that the widely spread points represented buildings constructed of concrete or brick. Notably, churches and other simplified buildings consisting of poles and a roof, which can be found in many parts of the islands, were likely to survive tsunami inundation with high flow depth and flow velocity. These simplified buildings consisting of poles and a roof are used as assembly halls in the Samoan Islands region. The tsunami flow passes under the roof of these simplified buildings, leaving most buildings of this type intact.

To validate the fragility functions, the number of destroyed buildings in each study area was estimated by multiplying the fragility functions by the corresponding tsunami features at each building locality. These values were compared, and accuracy rates were calculated for Pago Pago, Leone, Poloa and Amanave, as shown in Table 5. The fragility functions tended to underestimate the true damage by 10 to 20 %. These observations imply that buildings that are resilient against tsunami inundation, such as concrete buildings and Samoan-specific simplified buildings, caused the underestimation of the fragility functions. When these functions are applied in city planning, these features should be taken into account. In Pago Pago, Poloa, and Leone, the fragility functions of hydrodynamic force showed relatively greater accuracy. Therefore, the actual force that acts on the buildings should be given stronger consideration than the flow depth and current velocity. The accuracy rates for Amanave were lower than those for the other areas because the actual topographic conditions at Amanave differ from the DEM published by NOAA-NGDC, and we were unable to accurately reproduce the tsunami behavior in this area.

NHESSD
2, 1–25, 2014

6 Conclusion

In this study, tsunami fragility functions in terms of flow depth, flow velocity and hydrodynamic force were developed for American Samoa by integrating tsunami numerical modeling with remote-sensing technology.

The mechanism of tsunami generation was analyzed through numerical simulations. The waveforms measured by three DART gauges were reproduced well if the fault rupture on the interface was assumed to begin three minutes before the fault rupture on the outer rise. The tsunami-inundation distributions were then derived and validated using field-survey data.

The spatial distribution of building damage was interpreted by comparing pre- and post-tsunami high-resolution satellite images of the affected areas.

Finally, fragility functions were developed, and structural vulnerability in American Samoa was quantitatively evaluated. These functions were validated by estimating the number of destroyed buildings and comparing these estimates to the observed data.

Acknowledgements. This research was financially supported by the Industrial Technology Research Grant Program in 2008 (Project ID: 08E52010a) from the New Energy and Industrial Technology Development Organization (NEDO); by a Grant-in-Aid for Scientific Research (Project Number: 22681025) from the Ministry of Education, Culture, Sports, Science and Technology (MEXT); by a Grant-in-Aid for JSPS Fellows (Project Number: 24·5839) and by the emergency tsunami survey.

References

Aburaya, T. and Imamura, F.: The proposal of a tsunami run-up simulation using combined equivalent roughness, Annual Journal of Coastal Engineering, Japan Society of Civil Engineers, 49, 276–280, 2002 (in Japanese).

Aida, I.: Reliability of a tsunami source model derived from fault parameters, J. Phys. Earth, 26, 57–73, 1978.

NHESSD

2, 1–25, 2014

Apotsos, A., Gelfenbaum, G., Jaffe, B., Watt, S., Peck, B., Buckley, M., and Stevens, A.: Tsunami inundation and sediment transport in a sediment-limited embayment on American Samoa, Earth-Sci. Rev., 107, 1–11, 2011.

Beavan, J., Wang, X., Holden, C., Wilson, K., Power, W., Prasetya, G., Bevis, M., and Kautoke, R.: Near-simultaneous great earthquakes at Tongan megathrust and outer rise in September 2009, Nature, 466, 19, 2010.

Didenkulova, I.: Tsunami runup in narrow bays: the case of Samoa 2009 tsunami, Nat Hazards, 65, 1629–1636, 2013.

Dudley, W. C., Whitney, R., Faasisila, J., Jowitt, S. F. A., and Chan-Kau, M.: Learning from the victims: new physical and social science information about tsunamis from victims of the 29 September 2009 event in Samoa and American Samoa, Earth-Sci. Rev., 107, 201–206, 2011.

Fritz, H. M., Borrero, J. C., Synolakis, C. E., Okal, E. A., Weiss, R., Titov, V. V., Jaffe, B. E., Foteinis, S., Lynett, P. J., Chan, I., and Liu, P. L. F.: Insights on the 2009 South Pacific tsunami in Samoa and Tonga from field surveys and numerical simulations, Earth-Sci. Rev., 107, 66–75, 2011.

IOC, IHO and BODC: Centenary Edition of the GEBCO Digital Atlas, published on CD-ROM on behalf of the Intergovernmental Oceanographic Commission and the International Hydrographic Organization as part of the General Bathymetric Chart of the Oceans, British Oceanographic Data Centre, Liverpool, UK, 2003.

Jaffe, B. E., Gelfenbaum, G., Buckley, M. L., Watt, S., Apotsos, A., Stevens, A. W., and Richmond, B. M.: The limit of inundation of the 29 September 2009, tsunami on Tutuila, American Samoa, US Geological Survey, 2010.

Jaffe, B., Buckley, M., Richmond, B., Strotz, L., Etienne, S., Clark, K., Watt, S., Gelfenbaum, G., and Goff, J.: Flow speed estimated by inverse modeling of sandy sediment deposited by the 29 September 2009 tsunami near Satitoa, east Upolu, Samoa, Earth-Sci. Rev., 107, 23–37, 2011.

Koshimura, S., Nishimura, Y., Nakamura, Y., Namegaya, Y., Fryer, G. J., Akapo, A., Kong, L., and Vargo, D.: Field survey of the 2009 tsunami in American Samoa, Eos Trans. AGU, 90, Fall Meet. Suppl., Abstract U23F-07, 2009a.

Koshimura, S., Oie, T., Yanagisawa, H., and Imamura, F.: Developing fragility functions for tsunami damage estimation using numerical model and post-tsunami data from Banda Aceh, Indonesia, Coast. Eng. J., 51, 243–273, 2009b.

NHESSD

2, 1–25, 2014

Koshimura, S., Kayaba, S., and Matsuoka, M.: Integrated Approach to Assess the Impact of Tsunami Disaster, Safety, Reliability and Risk of Structures, Infrastructures and Engineering Systems, edited by: Furuta, Frangopol and Shinozuka, 2010.

Lamarche, G., Pelletier, B., and Goff, J.: Impact of the 29 September 2009 South Pacific tsunami on Wallis and Futuna, Mar. Geol., 271, 297–302, 2010.

Lay, T., Ammon, C. J., Kanamori, H., Rivera, L., Koper, K. D., and Hutko, A. R.: The 2009 Samoa-Tonga great earthquake triggered doublet, Nature, 466, 19, doi:10.1038/nature09214, 2010.

Mas, E., Koshimura, S., Suppasri, A., Matsuoka, M., Matsuyama, M., Yoshii, T., Jimenez, C., Yamazaki, F., and Imamura, F.: Developing Tsunami fragility curves using remote sensing and survey data of the 2010 Chilean Tsunami in Dichato, Nat. Hazards Earth Syst. Sci., 12, 2689–2697, doi:10.5194/nhess-12-2689-2012, 2012.

Miura, H., Wijeyewickrema, A., and Inoue, S.: Evaluation of tsunami damage in the eastern part of Sri Lanka due to the 2004 Sumatra earthquake using remote sensing technique, Proc. 8th National Conference on Earthquake Engineering, Paper No. 8, NCEE-856, 2006.

Namegaya, Y., Koshimura, S., Nishimura, Y., Nakamura, Y., Gerard, F., Akapo, A., and Kong, S. L.: A rapid-response field survey of the 2009 Samoa earthquake tsunami in American Samoa, Journal of Japan Society of Civil Engineers, Ser. B2 (Coastal Engineering), 66, 1366–1370, 2010 (in Japanese).

Okal, E. A., Fritz, H. M., Synolakis, C. E., Borrero, J. C., Weiss, R., Lynett, P. J., Titov, V. V., Foteinis, S., Jaffe, B. E., Liu, P. L. F., and Chan, I.: Field survey of the Samoa tsunami of 29 September 2009, Seismolog. Res. Lett., 81, 577–591, 2010.

Okal, E. A., Borrero, J. C., and Chagu-Goffé, C.: Tsunamigenic predecessors to the 2009 Samoa earthquake, Earth-Sci. Rev., 107, 128–140, 2011.

Reese, S., Bradley, B. A., Bind, J., Smart, G., Power, W., and Sturman, J.: Empirical building fragilities from observed damage in the 2009 South Pacific tsunami, Earth-Sci. Rev., 107, 156–173, 2011.

Roeber, V., Yamazaki, Y., and Cheung, K.F.: Resonance and impact of the 2009 Samoa tsunami around Tutuila, American Samoa, Geophys. Res. Lett., 37, L21604, doi:10.1029/2010GL044419, 2010.

Suppasri, A., Koshimura, S., and Imamura, F.: Developing tsunami fragility curves based on the satellite remote sensing and the numerical modeling of the 2004 Indian Ocean tsunami

NHESSD
2, 1–25, 2014

in Thailand, Nat. Hazards Earth Syst. Sci., 11, 173–189, doi:10.5194/nhess-11-173-2011, 2011.

Suppasri, A., Mas, E., Koshimura, S., and Imai, K.: Developing Tsunami Fragility Curves From the Surveyed Data of the 2011 Great East Japan Tsunami in Sendai and Ishinomaki Plains, Coast. Eng. J., 54, 1250008, doi:10.1142/S0578563412500088, 2012.

USGeological Survey: Earthquake Hazards Program, Magnitude 8.1 – SAMOA ISLANDS REGION, available at: http://earthquake.usgs.gov/earthquakes/eqinthenews/2009/us2009mdbi/#details, 2009.

van ZijlldeJong, S. L., Dominey-Howes, D., Roman, C. E., Calgaro, E., Gero, A., Veland, S., Bird, D. K., Muliaina, T., Tuiloma-Sua, D., Afioga, T. L.: Process, practice and priorities – key lessons learnt undertaking sensitive social reconnaissance research as part of an (UNESCO-IOC) International Tsunami Survey Team, Earth-Sci. Rev., 107, 174–192, 2011.

Wilson, R. I., Dengler, L. A., Goltz, J. D., Legg, M. R., Miller, K. M., Ritchie, A., and Whitmore, P. M.: Emergency response and field observation activities of geoscientists in California (USA) during the 29 September 2009, Samoa Tsunami, Earth-Sci. Rev., 107, 193–200, 2011.

NHESSD

2, 1–25, 2014

Table 1. Fault parameters used for far-field tsunami-propagation simulations.

Fault parameters	Outer rise 1	Outer rise 2	Interface
Lat (°)	−15.613	−15.842	−15.940
Long (°)	−171.859	−171.804	−172.718
Strike (°)	330	330	175
Dip (°)	48	48	16
Rake (°)	−150	−90	85
Length (km)	52.5	17.5	109
Width (km)	45	45	90
Area (km^2)	2362.5	743.75	9810
Depth (km)	13	13	18
Slip (m)	8.6	8.6	4.1
Time delay (sec)	0	0	−180
Rise time (sec)	60	60	480
Rigidity (Nm^{-2})	3.00E+10	3.00E+10	3.00E+10
Moment (Nm)	0.61E+21	0.19E+21	1.19E+21
M_w (total = 8.13)	7.79	7.45	7.98

NHESSD
2, 1–25, 2014

Table 2. Fault parameters used for the numerical models of tsunami inundation.

Parameter	Outer rise	Interface
Lat (°)	−15.542	−15.940
Lon (°)	−172.237	−172.718
Strike (°)	352	175
Dip (°)	48	16
Rake (°)	−41	85
Length (km)	114	109
Width (km)	28	90
Depth (km)	13	18
Slip (m) [PagoPago/Amanave/Poloa/Leone]	9.6/14.6/12.6/10.6	4.1/4.1/4.1/4.1
Rigidity (Nm^{-2})	3.00E+10	3.00E+10
Moment (Nm)	0.82E+21	1.19E+10
M_w	7.9	8.0

NHESSD
2, 1–25, 2014

Table 3. Building-damage interpretation results.

Damage category	Number of buildings [PagoPago/Amanave/Poloa/Leone/Total]
(a) Survived	54/34/4/196/288
(b) Major damage	14/2/0/12/28
(c) Collapsed	7/3/1/7/18
(d) Washed-away	34/42/13/28/117

NHESSD
2, 1–25, 2014

Table 4. Fragility-function parameters obtained from the regression analysis. R^2 is the coefficient of determination obtained by least-squares fitting.

x for fragility functions P(x)	μ	σ	λ	ξ	R^2
Flow depth (m)	N/A	N/A	1.17	0.69	0.89
Current velocity ($m\,s^{-1}$)	N/A	N/A	0.54	1.65	0.73
Hydrodynamic force per width ($kN\,m^{-1}$)	N/A	N/A	1.07	3.16	0.72

NHESSD
2, 1–25, 2014

Table 5. Numbers of destroyed buildings estimated by the developed fragility functions.

Study area	Tsunami feature	Estimated	Observed	Accuracy rate
Pago Pago	Flow depth	39.98	55	0.71
	Flow velocity	40.74		0.74
	Hydrodynamic force	39.97		0.73
Amanave	Flow depth	29.69	47	0.42
	Flow velocity	28.81		0.37
	Hydrodynamic force	29.12		0.39
Poloa	Flow depth	12.15	14	0.85
	Flow velocity	11.74		0.81
	Hydrodynamic force	12.64		0.89
Leone	Flow depth	37.62	47	0.75
	Flow velocity	55.59		0.85
	Hydrodynamic force	49.46		0.95
Total	Flow depth	118.54	163	0.62
	Flow velocity	136.88		0.81
	Hydrodynamic force	131.19		0.76

NHESSD
2, 1–25, 2014

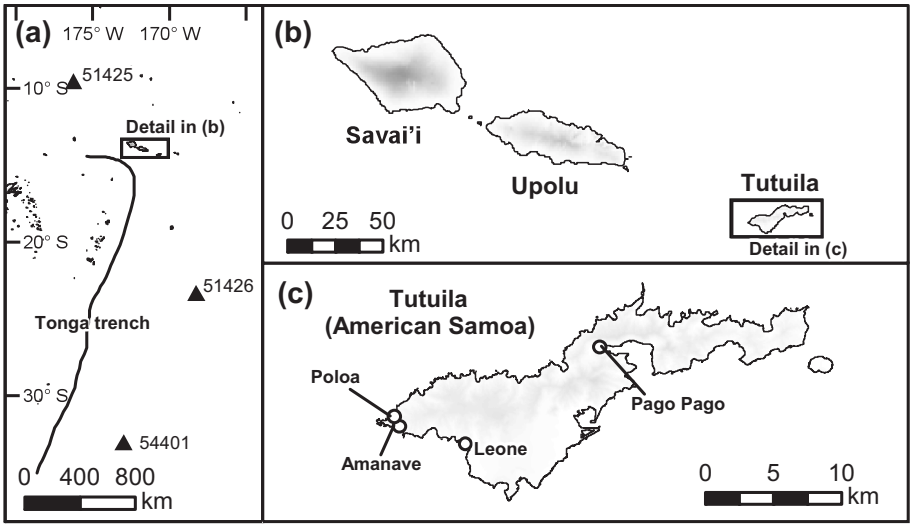

Fig. 1. Study area (Pago Pago, Leone, Poloa and Amanave, American Samoa).

NHESSD
2, 1–25, 2014

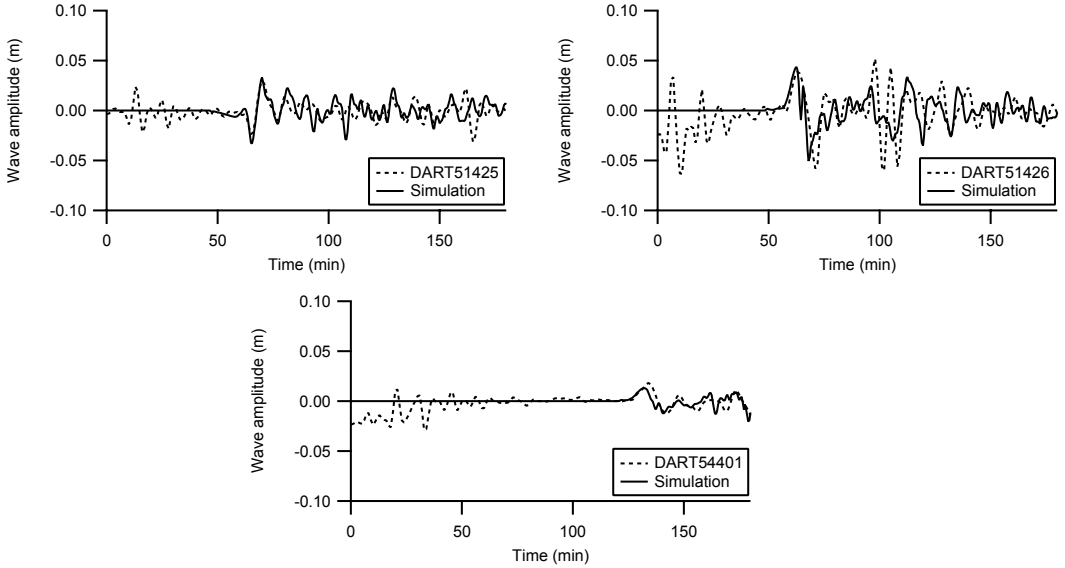

Fig. 2. Comparison of the modeled and observed waveforms at the DART gauges.

NHESSD
2, 1–25, 2014

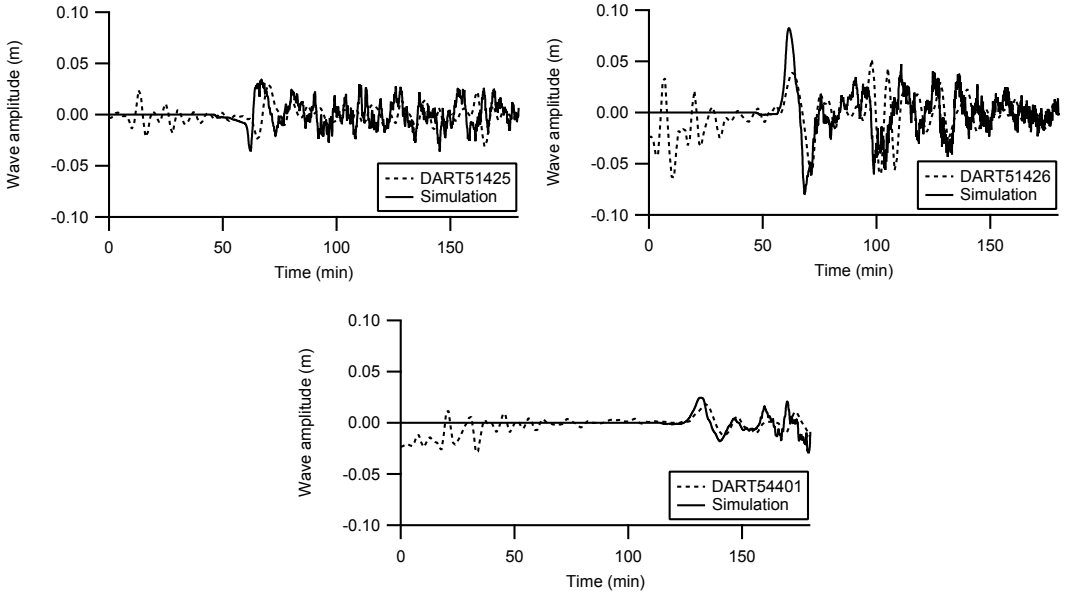

Fig. 3. Simulated waveforms used for tsunami-inundation models and observed waveforms at the DART gauges.

NHESSD
2, 1–25, 2014

Tsunami fragility functions for American Samoa

H. Gokon et al.

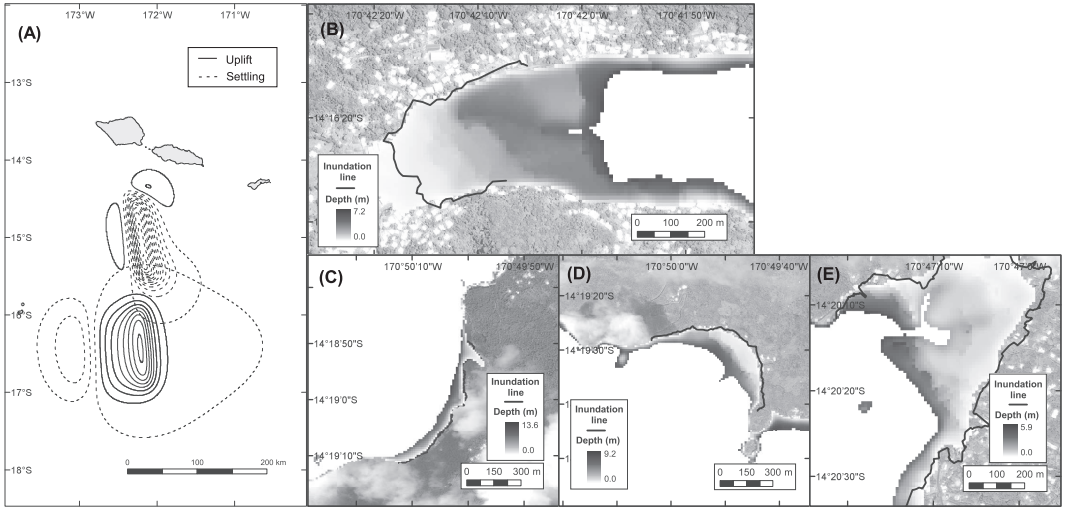

Fig. 4. (A) Tsunami source model used for tsunami-inundation simulations and examples of tsunami inundation at **(B)** Pago Pago, **(C)** Poloa, **(D)** Amanave, and **(E)** Leone.

NHESSD
2, 1–25, 2014

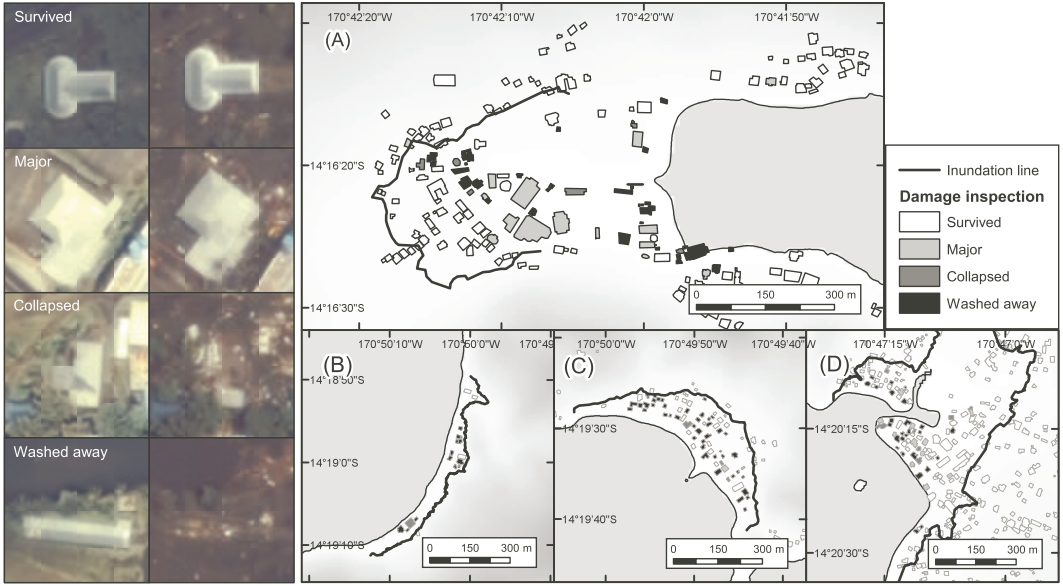

Fig. 5. Left: Classification criteria (left photo: pre-tsunami; right photo: post-tsunami). Right: Interpreted building damage at **(A)** Pago Pago, **(B)** Poloa, **(C)** Amanave and **(D)** Leone.

NHESSD
2, 1–25, 2014

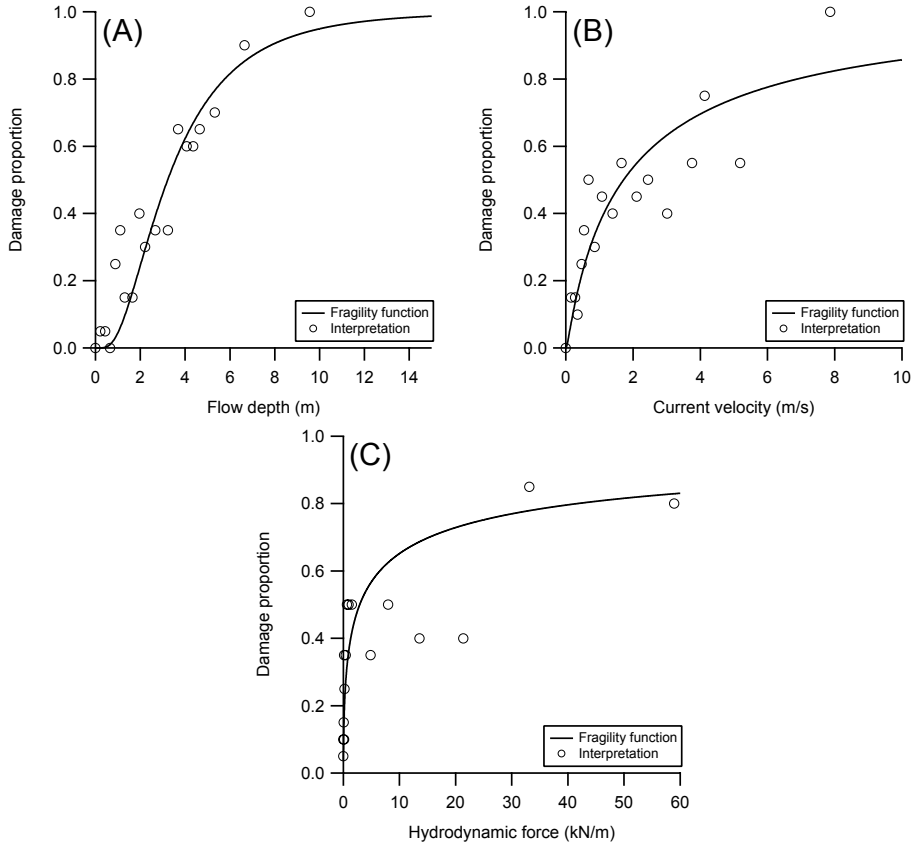

Fig. 6. Fragility functions of **(A)** flow depth, **(B)** current velocity, and **(C)** hydrodynamic force.

NHESSD
2, 1–25, 2014